

Subcritical Cracking of Modern 2¹/₄Cr-1Mo-¹/₄V Steel Due to Dissolved Internal Hydrogen and H₂ Environment, Research Report

API TECHNICAL REPORT 934-F, PART 3
FIRST EDITION, DECEMBER 2017



AMERICAN PETROLEUM INSTITUTE

Subcritical Cracking of Modern 2¹/₄Cr-1Mo-¹/₄V Steel Due to Dissolved Internal Hydrogen and H₂ Environment, Research Report

API TECHNICAL REPORT 934-F, PART 3
FIRST EDITION, DECEMBER 2017

Prepared under contract for API by:

Dr. Richard P. Gangloff
Emeritus Ferman W. Perry Professor of Materials Science and Engineering
Department of Materials Science and Engineering
School of Engineering and Applied Science
University of Virginia, Charlottesville, Virginia

Kevin Nibur, Ph.D., P.E.
Hy-Performance Testing, LLC
17676 Paladin Drive
Bend, OR 97701

Sylvain Pillot
Industeel, ArcelorMittal Group-Le Creusot Research Center
56 Rue Clémenceau – BP 19-F71201
Le Creusot, Cedex, France



AMERICAN PETROLEUM INSTITUTE

Special Notes

API publications necessarily address problems of a general nature. With respect to particular circumstances, local, state, and federal laws and regulations should be reviewed.

Neither API nor any of API's employees, subcontractors, consultants, committees, or other assignees make any warranty or representation, either express or implied, with respect to the accuracy, completeness, or usefulness of the information contained herein, or assume any liability or responsibility for any use, or the results of such use, of any information or process disclosed in this publication. Neither API nor any of API's employees, subcontractors, consultants, or other assignees represent that use of this publication would not infringe upon privately owned rights.

API publications may be used by anyone desiring to do so. Every effort has been made by the Institute to assure the accuracy and reliability of the data contained in them; however, the Institute makes no representation, warranty, or guarantee in connection with this publication and hereby expressly disclaims any liability or responsibility for loss or damage resulting from its use or for the violation of any authorities having jurisdiction with which this publication may conflict.

API publications are published to facilitate the broad availability of proven, sound engineering and operating practices. These publications are not intended to obviate the need for applying sound engineering judgment regarding when and where these publications should be utilized. The formulation and publication of API publications is not intended in any way to inhibit anyone from using any other practices.

Any manufacturer marking equipment or materials in conformance with the marking requirements of an API standard is solely responsible for complying with all the applicable requirements of that standard. API does not represent, warrant, or guarantee that such products do in fact conform to the applicable API standard.

Users of this technical report should not rely exclusively on the information contained in this document. Sound business, scientific, engineering, and safety judgment should be used in employing the information contained herein.

All rights reserved. No part of this work may be reproduced, translated, stored in a retrieval system, or transmitted by any means, electronic, mechanical, photocopying, recording, or otherwise, without prior written permission from the publisher. Contact the Publisher, API Publishing Services, 1220 L Street, NW, Washington, DC 20005.

Copyright © 2017 American Petroleum Institute

Foreword

Nothing contained in any API publication is to be construed as granting any right, by implication or otherwise, for the manufacture, sale, or use of any method, apparatus, or product covered by letters patent. Neither should anything contained in the publication be construed as insuring anyone against liability for infringement of letters patent.

Questions concerning the interpretation of the content of this publication or comments and questions concerning the procedures under which this publication was developed should be directed in writing to the Director of Standards, American Petroleum Institute, 1220 L Street, NW, Washington, DC 20005. Requests for permission to reproduce or translate all or any part of the material published herein should also be addressed to the director.

Generally, API standards are reviewed and revised, reaffirmed, or withdrawn at least every five years. A one-time extension of up to two years may be added to this review cycle. Status of the publication can be ascertained from the API Standards Department, telephone (202) 682-8000. A catalog of API publications and materials is published annually by API, 1220 L Street, NW, Washington, DC 20005.

Suggested revisions are invited and should be submitted to the Standards Department, API, 1220 L Street, NW, Washington, DC 20005, standards@api.org.

Contents

	Page
Executive Summary	xiv
Background	1
Literature Review of Hydrogen Cracking in Cr-Mo-V Steel	3
Research Objectives	4
Abbreviations	4
Experimental Procedures	4
Results	17
Discussion	93
Conclusions	136
Annex A—Cr-Mo-V Base Plate Specifications	139
Annex B—Cr-Mo-V Weld Metal Specifications	140
Bibliography	142
Figures	
1 The effect of predissolved bulk total H concentration on K_{IH} for IHAC of several heats of modern low-impurity Cr-Mo base plate and weld metal stressed under slow-rising K at 23 °C	2
2 Welded test block of 2¼Cr-1Mo-0.27V steel	6
3 Welded test block geometry	7
4 Autoclave assembly used for elevated-temperature H charging in a high-pressure H ₂ environment	8
5 The temperature dependence of the Sievert's law solubility coefficient for Cr-Mo and Cr-Mo-V steels	10
6 The temperature dependence of the H diffusivity for Cr-Mo and Cr-Mo-V steels	11
7 Results of an error analysis relating the concentration of dissolved H (top axis, in wppm) and the mass of the steel specimen analyzed (vertical axis, gm) to the error index	13
8 C(T) specimen orientation in the welded blocks of 2¼Cr-1Mo-¼V steel	14
9 Instrumentation elements of the IHAC test method	15
10 Compact tension specimen and associated probes for IHAC testing	16
11 Apparatus used for high-pressure H ₂ testing of compact tension specimens	18
12 Time-dependent H loss during isothermal exposure of 2¼Cr-1Mo-0.30V base metal in moist air at 23 °C and 100 °C	22
13 Time-dependent H loss during isothermal exposure of 2¼Cr-1Mo-0.27V weld metal in moist air at 23 °C and 100 °C	22
14 The temperature dependence of trap-sensitive effective H diffusivity (D_{H-Eff}) for weld metal and base plate of the 2¼Cr-1Mo-0.3V steel used in this API study of IHAC	23
15 R-curve based fracture toughness for step-cooled 2¼Cr-1Mo-0.3V base plate and weld metal at two loading temperatures	24

Contents

	Page
16 (Top) Load and DCPD vs CMOD, and (bottom) definition of the onset of stable crack propagation based on amplified DCPD vs CMOD	25
17 Scanning electron fractographs showing ductile fracture in 2¼Cr-1Mo-0.3V base metal at 23 °C	26
18 Crack extension vs applied K_J for C(T) specimens of 2¼Cr-1Mo-0.3V base metal, with and without precharged H	27
19 (Top left) DCPD vs CMOD and (bottom right) DCPD vs the J-integral to define the onset of crack extension at the indicated value of K_{IH} for specimen BM8A of 2¼Cr-1Mo-0.3V containing precharged H	28
20 (Top) Stretch zone in 2¼Cr-1Mo-0.3V base metal without H (BM2A), (bottom left) stretch zone appearance in a base metal specimen with precharged H (BM8A), and (bottom right) stretch zone in a H-precharged specimen of weld metal (WMA4)	29
21 The slope of DCPD vs CMOD, prior to the onset of organized crack extension, is parallel for noncharged base metal, noncharged weld metal, and H-precharged base metal at 26 °C and 40 °C	30
22 Measured DCPD vs CMOD (top) and calculated crack length from Johnson’s equation vs CMOD (bottom), using the first deviation in DCPD–CMOD linearity as the onset of crack extension for specimen BM6A	32
23 Measured DCPD vs CMOD (top) and calculated crack length from Johnson’s equation vs CMOD (bottom), using the first deviation in DCPD–CMOD linearity as the onset of crack extension for specimen BM10A	33
24 SEM fractographs of the zones of stretch and stable cracking ahead of the fatigue precrack shown in the bottom half of each image for: (top) BM6A and (bottom) BM10A	34
25 Measured DCPD vs CMOD (top) and calculated crack length from Johnson’s equation vs CMOD (bottom), using the first deviation in DCPD–CMOD linearity as the onset of crack extension for specimen BM4A	36
26 SEM fractograph of the zones of fatigue precrack (bottom arrow), stretch/H cracking (middle arrow), and post-test cleavage (top arrow) specimen BM4A	37
27 Measured DCPD vs CMOD (top) and SEM fractograph for specimen BM11A	38
28 Measured DCPD vs CMOD (top) and SEM fractograph for weld metal specimen WMC4	40
29 Measured DCPD vs CMOD (top) and calculated crack length from Johnson’s equation vs CMOD (bottom), using the indicated deviation in DCPD–CMOD linearity as the onset of crack extension for specimen WMD3	41
30 SEM fractograph of the three zones of cracking observed in the interrupted loading experiment with H-precharged weld metal specimen WMD3	42
31 Macrophotographs of the fracture surfaces for interrupted specimens of Cr-Mo-V steel	42
32 Measured DCPD vs CMOD (top) and calculated crack length from Johnson’s equation vs CMOD (bottom)	43
33 Composite SEM fractographs of the fracture surface from specimen BM12-3	44

Contents

	Page	
34	Macrophotographs of 2¼Cr-1Mo-0.30V base metal compact tension specimens that were fatigue precracked, H-precharged, stressed under slow-rising K in moist air, unloaded, and fractured in liquid nitrogen	48
35	(Top) Load and DCPD vs CMOD. (Middle) Amplified definition of the onset of crack propagation using the defined departure in linear DCPD vs CMOD at the resulting value of K_{IH} . (Bottom) Crack growth resistance curve, given as the amount of stable crack growth vs applied elastic-plastic K	49–50
36	Crack growth resistance curves, plotted as the elastic-plastic stress intensity factor vs crack extension from DCPD, for H-precharged 2¼Cr-1Mo-0.3V base metal stressed under slow-rising K at 26 °C.	51
37	Macrograph of the fracture surface of 2¼Cr-1Mo-0.3V base metal specimen BM8A, showing the fatigue precrack (bottom flat region), IHAC region (middle roughened features), and liquid nitrogen cleavage region (top)	52
38	Scanning electron fractographs for (top) ductile fracture in H-free 2¼Cr-1Mo-0.3V BM and (bottom) IHAC in H-precharged BM, each stressed under slow-rising K in moist air at 26 °C.	52
39	Scanning electron fractographs for (top left) ductile fracture in H-free 2¼Cr-1Mo-0.3V BM and (top right and bottom) IHAC in H-precharged BM, each stressed under slow-rising K in moist air at 26 °C	53
40	The loading rate dependence of K_{IH} for IHAC in 2¼Cr-1Mo-0.3V BM at 26 °C compared to values measured for 2¼Cr-1Mo BM and WM at 23 °C to 26 °C using the conservatively aggressive slow-rising K test method.	54
41	Crack growth resistance curves, plotted as crack extension vs the elastic-plastic stress intensity factor, for 2¼Cr-1Mo-0.30V base metal, both as-received and after H charging, for slow-rising K loading at a 23 °C and 100 °C	55
42	Crack growth resistance curves, plotted as the elastic-plastic stress intensity factor vs crack extension from DCPD, for H-precharged 2¼Cr-1Mo-0.3V base metal stressed under slow-rising K at a variety of temperatures	55
43	Crack growth resistance curves, plotted as the elastic-plastic stress intensity factor vs crack extension from DCPD, for H-precharged 2¼Cr-1Mo-0.3V base metal stressed under slow-rising K at a variety of temperatures	56
44	The temperature dependence of K_{IH} for IHAC in 2¼Cr-1Mo-0.3V BM for the specific slow-rising dK/dt and total remaining H concentration conditions listed in Table 9	56
45	The temperature dependencies of K_{IH} (○,● from Figure 44) and K_{JIH} (▲) for IHAC in 2¼Cr-1Mo-0.30V BM for the specific slow-rising dK/dt and total remaining H concentration conditions listed in Table 9	57
46	Crack growth resistance curve and C(T) specimen temperature vs crack extension for the H-precharged 2¼Cr-1Mo-0.30V BM specimen stressed under slow-rising K at –10 °C	58
47	Macrophotographs of fatigue precracked, H-precharged, and fractured specimens of 2¼Cr-1Mo-0.27V weld metal. (top) WMA4 and (bottom) WMA1	59

Contents

	Page
48 (Top) Load and DCPD vs CMOD. (Middle) Amplified definition of the onset of crack propagation using the defined departure in linear DCPD vs CMOD at the resulting value of K_{IH} . (Bottom) Crack growth resistance curve, given as the amount of stable crack growth vs applied elastic-plastic K	59–60
49 Applied elastic-plastic K_J vs stable crack extension for 2¼Cr-1Mo-0.27V weld metal subjected to slow-rising displacement loading at 26 °C, with and without H precharging to a total dissolved H concentration of between 7.5 wppm and 7.8 wppm remaining in the C(T) specimen after fracture testing.	61
50 SEM fractographs of the IHAC morphology in 2¼Cr-1Mo-0.27V weld metal (specimen WMA4: 26 °C, 7.8 wppm remaining H content, 18 MPa√m/h) showing the region just after the fatigue precrack, with H-assisted crack propagation from bottom to top.	63
51 SEM fractographs of the IHAC morphology in 2¼Cr-1Mo-0.27V weld metal (specimen WMA4: 26 °C, 7.8 wppm remaining H content, 18 MPa√m/h) showing the region substantially ahead of the fatigue precrack, with H-assisted crack propagation from bottom to top . .	64
52 SEM fractographs of the IHAC morphology in 2¼Cr-1Mo-0.27V weld metal (specimen WMA4: 26 °C, 7.8 wppm remaining H content, 18 MPa√m/h) showing the region substantially ahead of the fatigue precrack, with H-assisted crack propagation from bottom to top . . .	65
53 SEM fractographs of transgranular IHAC morphologies in 2¼Cr-1Mo-0.3V weld metal (left images: specimen WMA4: 26 °C, 7.8 wppm remaining H content, 18 MPa√m/h) and base metal (right images: specimen BM8A 25 °C, 9.5 wppm remaining H content, 2 MPa√m/h) comparing various regions ahead of the fatigue precrack, with H-assisted crack propagation from bottom to top	66
54 Applied elastic-plastic K_J vs stable crack extension for 2¼Cr-1Mo-0.27V weld metal subjected to slow-rising displacement loading at 26 °C and 100 °C, with and without H precharging to a total dissolved H concentration of between 7.5 wppm and 7.8 wppm for 26 °C and 6.6 wppm for the 100 °C specimen	67
55 Crack growth resistance curves, plotted as the elastic-plastic stress intensity factor vs crack extension from DCPD, for H-precharged 2¼Cr-1Mo-0.27V weld metal stressed under slow-rising K at a variety of temperatures	67
56 The temperature dependence of K_{IH} for IHAC in 2¼Cr-1Mo-0.27V WM for the specific slow-rising dK/dt and total remaining H concentration conditions listed in Table 9	68
57 The temperature dependence of K_{JIH} for IHAC in 2¼Cr-1Mo-0.27V WM for the specific slow-rising dK/dt and total remaining H concentration conditions listed in Table 9	69
58 Applied elastic-plastic K_J vs stable crack extension for 2¼Cr-1Mo-0.3V base metal and weld metal, each subjected to slow-rising displacement loading at 26 °C and 100 °C, with and without precharging to the indicated total dissolved H concentrations.	70
59 Crack growth resistance for the API lot of 2¼Cr-1Mo-0.3V BM tested in high-pressure H_2 (25 °C) at Sandia National Laboratory in Livermore, CA, compared to the behavior of H-free and H-precharged specimens tested at Hy-Performance Materials Testing	71
60 (Top) Load and DCPD vs CMOD. (Middle) Amplified definition of the onset of crack propagation using the defined departure in linear DCPD vs CMOD at the resulting value of K_{IH} . (Bottom) Crack growth resistance curve, given as the amount of stable crack growth vs applied elastic-plastic K	72–73

Contents

Page

61	Elastic-plastic K_J vs Δa resistance curve for as-received 2¼Cr-1Mo-0.30V base metal stressed under slow-rising K in high-pressure H_2 at 25 °C and various P_{H_2} levels	74
62	Elastic-plastic K_J vs a resistance curve for as-received 2¼Cr-1Mo-0.30V base metal stressed under slow-rising K in high-pressure H_2 at 25 °C and various P_{H_2} levels, compared to the IHAC behavior of this base metal containing 9.5 wppm H-precharged H and stressed in moist air	75
63	Scanning electron fractographs of crack surfaces produced in 2¼Cr-1Mo-0.30V base metal stressed under slow-rising K in: (top left) moist air without H precharging, (b) moist air after H precharging, (c) high-purity low-pressure H_2 without H precharging, and (d) high-pressure H_2 without H precharging; each at 25 °C	76
64	Scanning electron fractographs of crack surfaces produced in 2¼Cr-1Mo-0.30V base metal stressed under slow-rising K in: (top left) moist air without H precharging, (b) moist air after H precharging, (c) high-purity, low-pressure H_2 without H precharging, and (d) high-pressure H_2 without H precharging; each at 25 °C	77
65	H_2 pressure dependence of K_{IH} for slow-rising K stressing of as-received 2¼Cr-1Mo-0.3V base metal and weld metal for a variety of environmental conditions discussed in the text. The H-free K_{JICi} is arbitrarily plotted at P_{H_2} of 0.001 MPa, and the regression equation is shown based on the data for BM in pure H_2 at 25 °C (●), without K_{JICi} (top) and with K_{JICi} (bottom) . .	78
66	H_2 pressure dependence of K_{JIH} for slow-rising K stressing of as-received 2¼Cr-1Mo-0.3V base metal and weld metal for a variety of environmental conditions discussed in the text. The H-free K_{JIC} is plotted at 0.001 MPa, and the regression equation is shown based on the data for BM in pure H_2 at 25 °C (●) with K_{JIC}	79
67	Elastic-plastic K_J vs Δa resistance curve for as-received 2¼Cr-1Mo-0.30V base metal stressed under slow-rising K in high-pressure H_2 , and in O_2 -contaminated H_2 , each at 25 °C and P_{H_2} of 13.8 MPa	80
68	Elastic-plastic K_J vs Δa resistance curves for as-received (0 wppm H) and H-precharged (9.3 wppm to 9.4 wppm H) 2¼Cr-1Mo-0.30V base metal stressed under slow-rising K in high-pressure H_2 (P_{H_2} of 4.8 MPa or 13.8 MPa), compared to the behavior of as-received as well as H-precharged (9.5 wppm) BM stressed in moist air, each at 25 °C	81
69	Elastic-plastic K_J vs Δa resistance curves for as-received (0 wppm H) and H-precharged (7.2 wppm to 7.8 wppm H) 2¼Cr-1Mo-0.27V weld metal stressed under slow-rising K in either moist air or 13.8 MPa H_2 , each at 25 °C	82
70	Elastic-plastic K_J vs Δa resistance curves for as-received (0 wppm H) 2¼Cr-1Mo-0.3V weld metal and base metal stressed under slow-rising K in moist air compared to results for H-precharged (7.2 wppm or 9.4 wppm H) WM and BM stressed in high-pressure H_2 (P_{H_2} of 13.8 MPa), each at 25 °C	83
71	H_2 pressure dependence of K_{IH} for slow-rising K stressing of as-received and H-precharged 2¼Cr-1Mo-0.3V base metal and weld metal for a variety of environmental conditions discussed in the text. The H-free K_{JICi} is arbitrarily plotted at P_{H_2} of 0.001 MPa, and the regression equation is shown based on the data for BM in pure H_2 at 25 °C (●), without K_{JICi} (top) and with K_{JICi} (bottom)	84

Contents

Page

72	H ₂ pressure dependence of K _{JIH} for slow-rising K stressing of as-received and H-precharged 2¼Cr-1Mo-0.3V base metal and weld metal for a variety of environmental conditions discussed in the text. The H-free K _{JIC} is plotted at 0.001 MPa and the regression equation is shown based on the data for BM in pure H ₂ at 25 °C (●) with K _{JIC}	85
73	Effect of loading format on the IHAC growth rate vs stress intensity factor relationship for a modern-pure 2¼ Cr-1Mo base plate containing 5 wppm predissolved H (C _{H-Total}) and stressed at 23 °C	86
74	Crack length vs time for a 2¼Cr-1Mo-0.30V base metal compact tension specimen, precharged with H and stressed in moist air under slow-rising CMOD to induce stable-subcritical IHAC at 25 °C, followed by application of a CMOD hold period starting at 84 h and ending at 90.7 h	87
75	Crack growth rate vs elastic-plastic stress intensity factor, analyzed using the data in Figure 74 for a 2¼Cr-1Mo-0.30V base metal compact tension specimen, precharged with H and stressed in moist air under slow-rising CMOD to induce stable-subcritical IHAC at 25 °C, followed by application of a CMOD hold period starting at 84 h	88
76	Crack length vs time for a 2¼Cr-1Mo-0.30V base metal compact tension specimen, precharged with H and stressed in moist air under slow-rising CMOD to induce stable-subcritical IHAC at 100 °C, followed by application of a CMOD hold period starting at 61.4 h and ending at 65.4 h	89
77	Crack length vs time for a 2¼Cr-1Mo-0.27V weld metal compact tension specimen, precharged with H and stressed in moist air under slow-rising CMOD to induce stable-subcritical IHAC at 26 °C, followed by application of a CMOD hold period starting at 26.8 h and ending at 34.1 h	90
78	Crack length vs time for a 2¼Cr-1Mo-0.27V weld metal compact tension specimen, precharged with H and stressed in moist air under slow-rising CMOD to induce stable-subcritical IHAC at 100 °C, followed by application of a CMOD hold period starting at 26.5 h and ending at 35.1 h	91
79	Crack length vs time for a 2¼Cr-1Mo-0.30V base metal compact tension specimen, stressed under slow-rising CMOD in 13.8 MPa H ₂ without H precharging to induce stable-subcritical HEAC at 25 °C, followed by application of a CMOD hold period starting at 15.4 h and ending at 18 h	92
80	Crack length vs time for a 2¼Cr-1Mo-0.30V base metal compact tension specimen, precharged with H and stressed under slow-rising CMOD in 13.8 MPa H ₂ to induce table-subcritical HEAC at 25 °C, followed by application of a CMOD hold period starting at 15.3 h and ending at 18.3 h	93
81	The loading rate dependence of K _{IH} for IHAC in 2¼Cr-1Mo-0.3V BM at 26 °C compared to values measured for 2¼Cr-1Mo BM and WM at 23 °C to 26 °C using the conservatively aggressive slow-rising K test method	95
82	The total bulk-dissolved H concentration dependence of K _{IH} for IHAC in modern low J-factor 2¼Cr-1Mo BM and WM, compared to that for 2¼Cr-1Mo-0.30V base metal from the present study. Each K _{IH} was measured using the slow-rising K test protocol. Test temperature was 23 °C for Cr-Mo and between -10 °C and 122 °C for Cr-Mo-V base metal, with specific test conditions and results given in Table 9.	96

Contents

Page

83	The total bulk-dissolved H concentration dependence of K_{IH} for IHAC in modern low J-factor 2¼Cr-1Mo BM and WM, compared to that for 2¼Cr-1Mo-0.27V weld metal from the present study. Each K_{IH} was measured using the slow-rising K test protocol. Test temperature was 23 °C for Cr-Mo and between -10 °C and 140 °C for Cr-Mo-V, with specific test conditions and results given in Table 9	96
84	Scanning electron fractographs showing: (top left) microvoid-based ductile fracture in specimen BM2A that was fractured in moist air without H precharging, (top right) transgranular IHAC in specimen BM8A, and (bottom left and right) transgranular IHAC in WM4A	97
85	The effect of test temperature on K_{IH} for the onset of IHAC under rising CMOD ($dK/dt = 0.007 \text{ MPa}\sqrt{\text{m}}$) for 2¼Cr-1Mo base plate and weld metal of moderate-purity and a single $C_{H\text{-Total}}$ of 5 wppm	98
86	The temperature dependence of K_{IH} for IHAC in 2¼Cr-1Mo-0.3V base plate and weld metal for the specific slow-rising dK/dt and total remaining H concentration conditions listed in Table 9.	99
87	The temperature dependence of K_{JIH} for IHAC in 2¼Cr-1Mo-0.3V base plate and weld metal for the specific slow-rising dK/dt and total remaining H concentration conditions listed in Table 9.	100
88	The temperature dependence of K_{IH} for IHAC in 2¼Cr-1Mo base metal from Figure 85, compared to K_{IH} for 2¼Cr-1Mo-0.30V BM for the slow-rising dK/dt and total remaining H concentration conditions listed in Table 9	101
89	The temperature dependence of K_{IH} for IHAC in 2¼Cr-1Mo base metal from Figure 85, compared to K_{IH} and the 0.2 mm blunting line offset K_{JIH} for 2¼Cr-1Mo-0.30V BM for the slow-rising dK/dt and total remaining H concentration conditions listed in Table 9	102
90	The temperature dependence of K_{IH} for IHAC in 2¼Cr-1Mo weld metal from Figure 85, compared to K_{IH} for 2¼Cr-1Mo-0.27V WM for the slow-rising dK/dt and total remaining H concentration conditions listed in Table 9	103
91	The temperature dependence of K_{IH} for IHAC in 2¼Cr-1Mo weld metal from Figure 85, compared to K_{IH} and the 0.2 mm blunting line offset K_{JIH} for 2¼Cr-1Mo-0.27V WM for the slow-rising dK/dt and total remaining H concentration conditions listed in Table 9	104
92	The temperature dependence of K_{IH} for IHAC in 2¼Cr-1Mo base metal and weld metal from Figure 85, compared to K_{IH} for 2¼Cr-1Mo-0.3V BM and WM for the slow-rising dK/dt and total remaining H concentration conditions listed in Table 9	105
93	H ₂ pressure dependence of K_{IH} for slow-rising K stressing of as-received 2¼Cr-1Mo-0.30V base metal for a variety of high-pressure H ₂ environmental conditions. The K_{JICi} for a H-free C(T) specimen is arbitrarily plotted at P_{H_2} of 0.001 MPa, and the regression is shown based on the three data points for BM in pure H ₂ at 25 °C (●)	106
94	The H ₂ pressure dependence of the threshold stress intensity for HEAC of alloy and C-Mn steels stressed at 25 °C	107
95	The temperature dependence of the threshold stress intensity for HEAC in several high and ultra-high strength martensitic steels tested in purified H ₂ at either constant or rising load . .	108

Contents

	Page
96 The loading rate dependence of the threshold stress intensity for IHAC (O) and HEAC (●, Δ) in H-precharged (4.4 wppm) Cr-Mo base metal stressed under slow-rising K in either moist air or high-pressure H ₂	109
97 The H ₂ pressure dependence of the threshold stress intensity for HEAC of alloy and C-Mn steels stressed at 25 °C	110
98 H ₂ pressure dependence of K _{IH} for slow-rising K stressing of as-received and H-precharged 2¼Cr-1Mo-0.3V base metal and weld metal	111
99 The H ₂ pressure dependence of the threshold stress intensity for HEAC of alloy and C-Mn steels stressed at 25 °C. Literature data for alloy steels (O) were obtained for quasi-static loading to yield a crack arrest threshold, while literature data for C-Mn steel (*, X; σ _{YS} = ~300 MPa) were obtained using the slow-rising K crack growth resistance curve method.	112
100 H ₂ pressure dependence of K _{JIH} for slow-rising K stressing of as-received and H-precharged 2¼Cr-1Mo-0.3V base metal and weld metal for a variety of environmental conditions discussed in the text	113
101 The H ₂ pressure dependence of the threshold stress intensity for HEAC of low alloy and C-Mn steels stressed at 25 °C. Literature data are described in the caption of Figure 99	114
102 The calculated effects of H ₂ pressure and H-trap binding energy on the fractional occupancy of H trap sites for isothermal exposure at 25 °C	116
103 <i>Open-system H Trapping.</i> The estimated exposure-temperature dependence of lattice-soluble H concentration (C _L) and reversibly trapped H concentration (C _T) for a single trap state described by a trap binding energy of 35 kJ/mole.	117
104 <i>Closed-system H Trapping.</i> The estimated cooling temperature dependence of lattice-soluble H concentration (C _L , ■ for high trap density and ● for low trap density) and reversibly trapped H concentration (C _T , solid lines) for a single trap state described by a trap binding energy of 35 kJ/mole	119
105 Model predictions of H partitioning among lattice sites and four trap site types for equilibrium exposure of 2¼Cr-1Mo steel to 18 MPa H ₂ at 450 °C	120
106 Model predictions of H partitioning among lattice sites and four trap site types for equilibrium exposure of 2¼Cr-1Mo and 2¼Cr-1Mo-0.3V steels to 18 MPa H ₂ at 450 °C, followed by cooling to 25 °C	121
107 The dependence of K _{IH} on crack tip C _{Tσ} , defined by Equation (1) at a location 9 μm ahead of the crack tip surface for: (top) moderate-purity/moderate-FATT Cr-Mo steel, and (bottom) high-purity/low-FATT Cr-Mo steel.	122
108 The effect of total dissolved H concentration (C _{H-Total-OP}), present during reactor operation, and crack tip diffusible H concentration (C _{H-Diff 470 μm}), localized at the reference point of δ _{470 μm} ahead of the crack tip, on the predicted critical temperature for elimination of IHAC in a cracked section fabricated from (top) moderate-purity/moderate 2¼Cr-1Mo steel and (bottom) high-purity/low-FATT 2¼Cr-1Mo steel, as a function of total H concentration in the bulk of the vessel wall during elevated temperature exposure in high-pressure H ₂	125
109 Potential effects of Cr-Mo-V characteristics on the critical temperature for the onset of slow-stable IHAC in V-modified Cr-Mo steel, as defined by Equation (2)	129

Contents

	Page
110 (Top) The total bulk-dissolved H concentration dependence of K_{IH} for IHAC in modern low J-factor 2¼Cr-1Mo BM and WM, compared to that for high-purity 2¼Cr-1Mo-0.3V base metal from the present study. (Bottom) The dependence of measured K_{IH} on crack tip H concentration defined by Equation (1) at a location 9 µm ahead of the crack tip surface high-purity/low-FATT Cr-Mo steel.	131
111 The effect of crack tip diffusible H concentration ($C_{H-Diff\ 470\ m}$), localized at the reference point of $\delta_{470\ m}$ ahead of the crack tip, on the predicted critical temperature for elimination of IHAC in a cracked section fabricated from high-purity 2¼Cr-1Mo ($\sigma_{YS} = 500\ MPa$) and 2¼Cr-1Mo-0.3V ($\sigma_{YS} = 575\ MPa$) steels following Equation (2) with $W_B = 38\ kJ/mol$, as a function of total H concentration dissolved in the bulk of the vessel wall during elevated temperature exposure in high-pressure H ₂	132
112 The effect of crack tip diffusible H concentration ($C_{H-Diff\ 470\ m}$), localized at the reference point of $\delta_{470\ \mu m}$ ahead of the crack tip, on the predicted critical temperature for elimination of IHAC in a cracked section fabricated from high-purity 2¼Cr-1Mo ($\sigma_{YS} = 500\ MPa$) and 2¼Cr-1Mo-0.3V ($\sigma_{YS} = 575\ MPa$) steels following Equation (2) with $E_B = 38\ kJ/mol$, as a function of total H concentration in the bulk of the vessel wall during elevated temperature exposure in high-pressure H ₂	133
113 The total bulk-dissolved H concentration dependence of K_{IH} for IHAC in modern low J-factor 2¼Cr-1Mo BM and WM [4,5], compared to that for 2¼Cr-1Mo-0.27V weld metal from the present study	134
114 The H ₂ pressure dependence of the threshold stress intensity for HEAC of alloy and C-Mn steels stressed at 25 °C	135
115 The effect of applied dK/dt , during rising CMOD, on the crack growth rate for IHAC in H-charged weld metal and base plate of 2¼Cr-1Mo steel, precharged with 5 wppm H and stressed at 25 °C	136

Tables

1 Modern Fracture Mechanics Characterization of the Rising-CMOD Threshold Stress Intensity for IHAC in Conventional and V-modified Cr-Mo Steel	3
2 Steel Composition	7
3 Steel Heat Treatment and Mechanical Properties	8
4 Sievert's Law Parameters for H Solubility in Cr-Mo and Cr-Mo-V Steels	9
5 Relationship Between Figure 7 Index, H Concentration, and Relative Error for Hot-extraction Measurements of H	12
6 Measurements of Total Dissolved Hydrogen Concentration in 2¼Cr-1Mo-0.3V Base Metal and Weld Metal	19
7 Measured H Concentrations After Isothermal Outgassing of 2¼Cr-1Mo-0.3V for the Indicated Time-Temperature Conditions	21
8 Interrupted IHAC Experiments	31
9 Fracture Experiment Results for 2¼Cr-1Mo-0.3V Base Plate and Weld Metal	45

EXECUTIVE SUMMARY

A literature review demonstrates the need for an improved laboratory database, as well as basic understanding, to quantitatively characterize the hydrogen-assisted cracking (HAC) resistance of modern 2¼Cr-1Mo-¼V base plate, weld metal, and the weld heat-affected zone. The objectives of this API-sponsored research are to: (a) quantitatively characterize the internal hydrogen-assisted cracking (IHAC) resistance of modern 2¼Cr-1Mo-¼V steel, in both base metal and weld metal product forms and including the effect of stressing temperature, (b) scope the hydrogen environment assisted cracking (HEAC) resistance of 2¼Cr-1Mo-¼V base metal, (c) understand the mechanism(s) for the IHAC and HEAC behaviors of Cr-Mo and Cr-Mo-V steels, centered on hydrogen (H) interactions with microstructure-scale trap sites, and (d) assess application of data and understanding of IHAC and HEAC to determine the role of subcritical H-assisted cracking on a minimum pressurization temperature (MPT) estimate relevant to thick-wall hydrotreating reactor vessels.

This work focused on slow-stable subcritical H cracking and did not examine the effect of H on the fracture toughness for unstable cracking. The temperature dependencies of IHAC of 2¼Cr-1Mo-0.3V base plate and weld metal were characterized using slow-rising displacement loading and elastic-plastic fracture mechanics analysis of crack growth measured through direct current potential difference (DCPD). This test method provides a conservative measure of susceptibility of alloy steels to HAC.

Specific conclusions of this research are as follows.

- 1) Compared to conventional 2¼Cr-1Mo steel, and consistent with the literature, the solubility of H dissolved in 2¼Cr-1Mo-0.3V base and weld metals increases two-fold due to VC precipitate trapping of H and when exposed to high-pressure H₂ at elevated temperature relevant to thick-wall reactor applications. Consistent with the reversible nature of H trapping at precipitate interfaces, the diffusivity of H in 2¼Cr-1Mo-0.3V decreases by about 100 times compared to H mobility in conventional 2¼Cr-1Mo steel.
- 2) Without predissolved H, the fracture resistance of high-purity (step-cooled) 2¼Cr-1Mo-0.3V base and weld metals is high at 25 °C and 100 °C, characteristic of upper shelf behavior and a fracture appearance transition temperature (FATT) well below room temperature.
- 3) Quantitative characterization of IHAC and HEAC in low- to moderate-strength steels is challenged by substantial crack tip plasticity. For 2¼Cr-1Mo-0.3V, the DCPD method, coupled with J-integral elastic-plastic fracture mechanics, effectively characterizes slow-stable H-assisted crack growth during slow-rising stress intensity factor loading. Measurement of the threshold for such cracking, K_{IH} , and the associated crack growth resistance curve as K_I vs Δa , are demonstrated to be conservative when based on DCPD vs crack mouth opening displacement (CMOD) analysis, rather than DCPD vs elastic-plastic J. A validated test protocol is now available at a commercial testing laboratory for use in fitness-for-service and MPT analyses where reactor-steel-specific H cracking properties are required.
- 4) Cr-Mo-V base and weld metals containing a high concentration of predissolved H, $C_{H-Total}$ of 6 wppm to 11 wppm from elevated temperature exposure in high-pressure H₂, significantly resist slow-stable IHAC compared to susceptible low-FATT (high-purity) Cr-Mo steel. Nonetheless, 2¼Cr-1Mo-0.3V is susceptible to slow-stable IHAC propagation for severe slow-rising displacement loading in moist air (see Figure 36).
- 5) 2¼Cr-1Mo-0.3V base metal (BM) and weld metal (WM) compact tension [C(T)] specimens exhibit stable crack extension that yields a rising R-curve, without evidence of the onset of H-stimulated premature fast fracture at K levels below K_{JIC} for H-free specimens. No evidence was obtained to demonstrate that H promotes premature fast fracture in these V-modified steels for the dissolved H concentration, loading rate, and temperatures examined. These results suggest that the H-stimulated fast fracture mechanism may not be operative in V-modified steel with a low FATT. This form of H degradation was reported in the literature to occur in Cr-Mo steel.

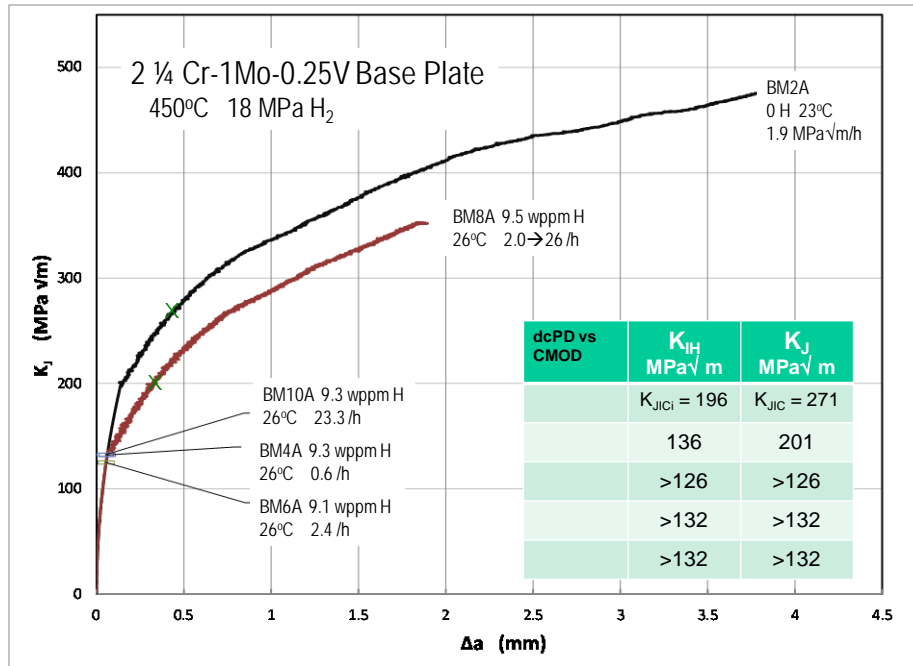


Figure 36—Crack growth resistance curves, plotted as the elastic-plastic stress intensity factor vs crack extension from DCPD, for H-precharged 2¼Cr-1Mo-0.3V base metal stressed under slow-rising K at 26 °C. Values of the 0.2 mm offset K_{JIH} and K_{JIC} are indicated by “X” on each resistance curve.

- 6) 2¼Cr-1Mo-0.27V weld metal is more susceptible to IHAC than 2¼Cr-1Mo-0.30V base metal, with the potential for variability in K_{IH} and K_J–Δa (see Figure 81, as well as Figures 82 and 83).

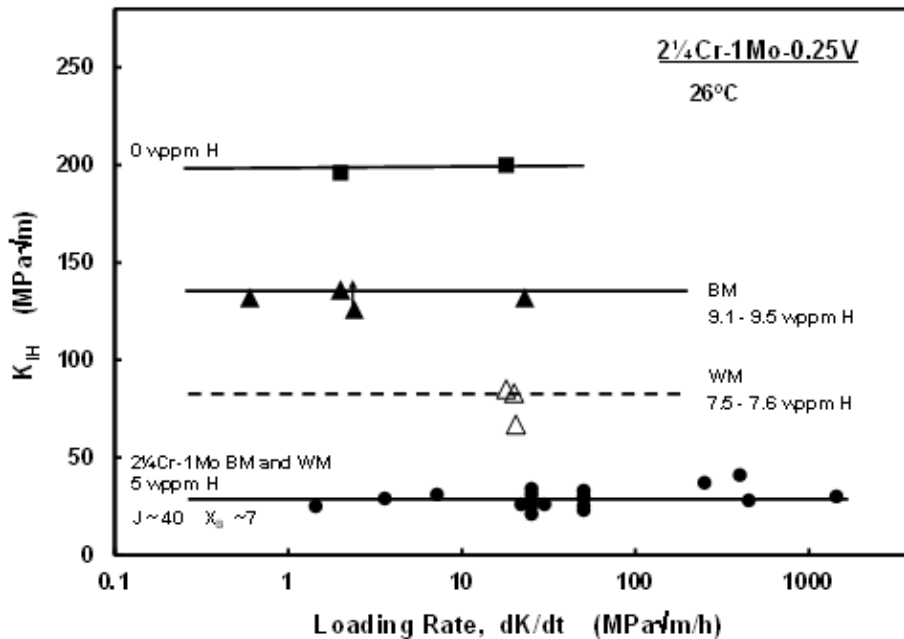


Figure 81—The loading rate dependence of K_{IH} for IHAC in 2¼Cr-1Mo-0.3V BM at 26 °C compared to values measured for 2¼Cr-1Mo BM and WM at 23 °C to 26 °C using the conservatively aggressive slow-rising K test method [2,4,5]. The conditions for the Cr-Mo steel experiments are reported in Bibliographic Item [2]. The dK/dt is the value of elastic K increase up to K_{IH}, above which this rate rises due to the onset of stable crack growth and/or plasticity.